

Acoustic Multifunctional Logic Gates and Amplifier based on Parity-Time Symmetry

Jun Lan^{1,*}, Liwei Wang^{1,*}, Xiaowei Zhang¹, Xiaozhou Liu^{1,a)}, Minghui Lu²

¹Key Laboratory of Modern Acoustics, Institute of Acoustics and School of Physics,
Collaborative Innovation Center of Advanced Microstructures, Nanjing University, Nanjing
210093, P. R. China.

²National Laboratory of Solid State Microstructures and Department of Materials Science
and Engineering, Nanjing University, Nanjing, 210093, P. R. China.

Acoustic analogue computation and signal processing are of great significance, however, it's challenging to realize the acoustic computing devices because of their limitation of single function and complex structure. The reveal of time-reversal property in the parity-time symmetric acoustic metamaterials has possibility to overcome those disadvantages and provide a new approach to realize multifunctional acoustic analogue computing device. In this paper, we theoretically and experimentally realize an acoustic multifunctional device which can gate and amplify acoustic waves at the same frequency using a passive acoustic parity-time symmetric metamaterial. The metamaterial is constructed by five lossless-loss periodically distributed structures. The interplay between the lossless and loss media is modulated to achieve the nearly parity-time symmetry. At the broken parity-time symmetry phase, the logic gates (XOR, OR, AND and NOT) and small signal amplifier are theoretically and experimentally realized at the same frequency by adjusting the phase and amplitude differences between the two incoming beams, respectively. Our work provides a new route for the connection between the parity-time symmetry and the metamaterial, which has great potential application in acoustic modulation and acoustic signal processing devices.

In optics, the realization of lasing and anti-lasing in a single system has opened up possibilities for optical multifunctional devices^{1,2}. Computational metastructure based on electromagnetic signals provides more efficient designs for analogy consumption³. Similar devices introduced into acoustics are of vital importance in the development of the efficient information processing and

*These authors contributed equally to this work.

^aEmail: xzliu@nju.edu.cn

reducing the integration complexity. Acoustic computing devices such as acoustic switches^{4,5}, diodes⁶, and logic gates^{7,8}, are central elements of acoustic computing and communication, and have attracted extensive attention. However, the realization of multiple functions coexisting without resorting to altering frequency and structure in these acoustic computing devices is a significant challenge. Many acoustic computing devices have been proposed relying on phononic metamaterials (PMs), which can control the propagation states of acoustic waves well by using the band gaps and distinct frequency characteristics^{9,10}. PMs are periodic structures composed of unit cells with different elastic properties. So far, acoustic computing devices based on PMs can be realized by means of the self-collimation effect⁷, the control waves¹¹, the rotating the rods of PMs¹² or the phase-control of incident waves¹³. However, most of them suffer simple functionality, complex design, or high-power consumption. It is also challenging to realize acoustic multifunctional devices at the same frequency. Therefore, it is necessary to seek for a simple and effective approach to design acoustic multifunctional devices that can tackle the above issues.

Meanwhile, Parity-time (*PT*) symmetry has grown into a burgeoning research area in acoustics. *PT* symmetry is initially proposed as a concept in the area of quantum mechanics^{14,15}. It has shown that the special class of Hamiltonians that commute with *PT* operator can exhibit entirely real energy eigenvalues even though they are non-Hermitian. Then, *PT* symmetry is extended to classical wave phenomena and its counterparts in the fields of optics, electronics and acoustics have been also found¹⁶⁻²⁰. The *PT* symmetric condition requires the real part of the refractive index modulation to be symmetric $n_R(x) = n_R(-x)$ and the imaginary part of the refractive index to be anti-symmetric $n_I(x) = -n_I(-x)$ ¹⁸. Exceptional point (EP) is a singular point of the eigenvalues and eigenvectors of the non-Hermitian system, where a spontaneous *PT* symmetry breaking can occur and the phase of transmission and reflection dislocates²¹⁻²³. A flurry of recent studies have demonstrated unique phenomena associated with the EP. The unique property of EP is usually utilized in non-Hermitian systems²⁴⁻²⁶. Through judiciously balancing the gain and loss regions of the *PT* symmetric system, a number of new applications have been explored, such as unidirectional invisibility^{17,27}, reflectionlessness²⁸⁻³⁰, coherent perfect absorber^{1,31-33} and laser^{2,34-36}. To realize *PT* symmetry in acoustic metamaterials, one must overcome the challenges associated with the absence of acoustic gain medium in nature³⁷. Recently, the passive acoustic *PT* symmetric metamaterials have been theoretically and experimentally demonstrated to realize the unidirectional sound focusing effect at

the EP^{28,38}. This provides us opportunities to investigate passive acoustic metamaterials with intrinsic PT symmetry and a variety of wave phenomena associated with EP or broken PT symmetry phase.

Inspired by these recent developments, we theoretically and experimentally realize a passive acoustic PT symmetric metamaterial, where the logic gates and amplifier at the same frequency are demonstrated in a single structure. PT symmetry ensures these two states occur at the same frequency. The acoustic PT symmetric metamaterial behaves like a distributed Bragg reflector which is composed of five lossless-loss periodically distributed structures, and the lengths of the lossless and loss structures are both one-quarter wavelength. The acoustic multifunctional device achieved here utilizes a highly efficient coherent control strategy based on PT symmetry. The refractive indices of the loss and lossless structures are carefully engineered by the scattering matrix formalism. In the broken PT symmetry phase, we theoretically and experimentally realize both logic gates and amplifier by controlling the initial phase of the two incident waves.

Results

Theoretical design to obtain passive PT symmetric system

In acoustics, a PT symmetric system with symmetrically distributed real part of refractive index $n_R(x) = n_R(-x)$ and anti-symmetrically distributed imaginary part of refractive index $n_I(x) = -n_I(-x)$ can be designed. As depicted in Fig. 1a, the passive acoustic PT symmetric system is composed of two types of periodically arranged cells A and B , which can be equivalent to a distributed Bragg reflector. The lengths of A and B are both one-quarter wavelength $l = \lambda_0/4 = 25$ mm and the total length of the PT symmetric structure is 250 mm. A is the acoustic lossless region with a real refractive index and B is the acoustic loss region with a complex refractive index whose imaginary part is negative. The lossless-loss PT symmetric modulation of the refractive index in each unit cell is given by

$$\begin{cases} n(x) = n_0 & (m-3.5)L \leq x \leq (m-3)L \\ n(x) = n_0 - 0.05\delta i & (m-3)L \leq x \leq (m-2.5)L \end{cases} \quad (1)$$

where $m = 1, 2, 3, 4, 5$; $n_0 = 1$ and δ denote the background refractive index and the lossless-loss factor, respectively. δ can be tuned from 0 to positive. x is the distance along the acoustic wave propagation direction and $L = \lambda_0/2 = 50$ mm is the Bragg period corresponding to half of the wavelength in the air at the operating frequency. Here, the operating frequency is the Bragg

frequency $f_B = 3430$ Hz . The real and imaginary parts of the refractive index distributed along the x direction are shown in Fig. 1b. The real part (red solid line) is an even function with respect to the position $x = 0$, while the imaginary part (black dotted line) is an odd function. Therefore, the lossless-loss system respects PT symmetry condition.

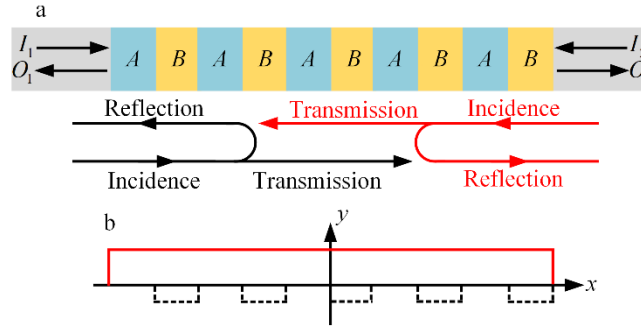


Figure 1| Passive acoustic PT symmetric system for acoustic multifunctional device. (a) Arrangement of the lossless medium (A region) and loss medium (B region) of the passive PT symmetric system. (b) The lossless-loss PT symmetric modulation of the real part (red solid line) and imaginary part (black dotted line) of the refractive index.

Operating principle and structure fabrication

In our work, an acoustic wave with another acoustic wave based on the coherent interaction of acoustic beams can be efficiently controlled. When the acoustic modulation satisfies the PT symmetry condition, the magnitudes of the transmission and left- (right-) reflection coefficients for the left (right) incidence must be the same, so that the interaction of the two coherent waves could vary continuously from 0 to a limit value. The limit value will be calculated later. Thus, by tuning the initial phase and amplitude differences between the two incident signals, the logic gates and small signal amplifier can be realized, respectively. As shown in Fig. 1a, the passive acoustic PT symmetric system is a two-port input/output system. The transfer matrix method in acoustics can be used to derive the acoustic scattering matrix describing the relation between the input and output acoustic waves, i.e.,
$$\begin{pmatrix} O_1 \\ O_2 \end{pmatrix} = \begin{pmatrix} t & r_L \\ r_R & t \end{pmatrix} \begin{pmatrix} I_2 \\ I_1 \end{pmatrix},$$
 where I_1 and I_2 are the amplitudes of the incident waves from the left and right ports, respectively. O_1 and O_2 are the amplitudes of the output waves at the left and right ports, respectively, which are the superposition of the transmission and reflection waves. $r_{L(R)}$ and t are the left-(right-) reflection and transmission coefficients, respectively. t is identical for both left and right incidences, due to reciprocity. Based on the transfer matrix method,

at the operating frequency $f_B = 3430$ Hz , the amplitudes of the transmitted and reflected waves at the left and right ports can be calculated by varying the lossless-loss factor δ , as shown in Fig. 2a. The amplitudes of t, r_L and r_R are the same when $\delta=3.335$. This is the necessary condition for the coherent interaction of two acoustic beams. According to Eq. (1), the material parameters (mass density and acoustic velocity) for the lossless A and loss B regions are $\rho_A = 1.21$ kg/m³ , $c_A = 343$ m/s , $\rho_B = 1.21$ kg/m³ and $c_B = 333.72 + 55.648i$ m/s , respectively. In the case of $\delta=3.335$, the amplitudes of the transmitted, and reflected waves at the left and right ports as functions of frequency are presented in Fig. 2b. It shows that at the frequency $f = 3430$ Hz, the left and right reflection and transmission coefficients are all around 0.34. Furthermore, the two associated eigenvalues of scattering matrix $S = \begin{pmatrix} t & r_L \\ r_R & t \end{pmatrix}$ are subsequently derived as $\lambda_{1,2} = t \pm \sqrt{r_L r_R}$. Figure 2c shows the absolute values of the two eigenvalues $|\lambda_{1,2}|$ as a function of frequency. It is worth mentioning that there exists a singular point at the operating frequency $f = 3430$ Hz, where the absolute values of the two associated eigenvalues of S go to either zero or the limit value (around 0.68), corresponding to the state of broken PT symmetry phase. In our passive PT symmetric system, this singular point is similar to the coherent perfect absorber-laser (CPAL) point of the active PT symmetric electromagnetic system, which simultaneously corresponds to the coherent perfect absorber mode and the lasing mode¹. Here, for our passive PT symmetric system, similar coherent perfect absorber mode and strong scattering mode (i.e. limited lasing mode, which is due to the lack of gain medium) simultaneously exist at this singular point. The calculated phases of the transmitted waves and the left- and right-reflected waves propagating through the designed passive PT symmetric system are shown in Fig. 2d. At the operating frequency $f = 3430$ Hz, there is π phase difference between the two reflections, and the phase difference between the transmission and reflections of the two ports is $\pm \pi/2$. Therefore, the ingeniously-designed lossless and loss regions of our passive PT symmetry system still possesses physical characteristics of the PT symmetry. By adjusting the phase difference of the two incident acoustic waves, the logic gates such as XOR, OR, AND and NOT can be achieved. Remarkably, Fig. 2 indicates that the realization of the broken PT symmetry phase creates two mutually opposite states: when the phase difference between the two beams is $\Delta\phi = \phi_1 - \phi_2 = -\pi/2$, acoustic wave becomes localized in the loss regions B , and the amplitude of the

output acoustic waves is approximately 0, corresponding to the output logic state 0. This presents the foundation to realize XOR and NOT gates with a high contrast ratio. ϕ_1 and ϕ_2 are the initial phases of the left and right incident beams, respectively. When the phase difference between two beams is $\Delta\phi = \phi_1 - \phi_2 = \pi/2$, acoustic wave is interferometrically confined in the lossless regions and the outgoing beams are resonantly amplified. By appropriately selecting the thresholds, the proposed device can function as an AND gate. Compared with the conventional acoustic coherent perfect absorption devices which only absorb the in-phase beams $\Delta\phi = 0$, the out-phase beams can be absorbed by the introduction of PT symmetry.

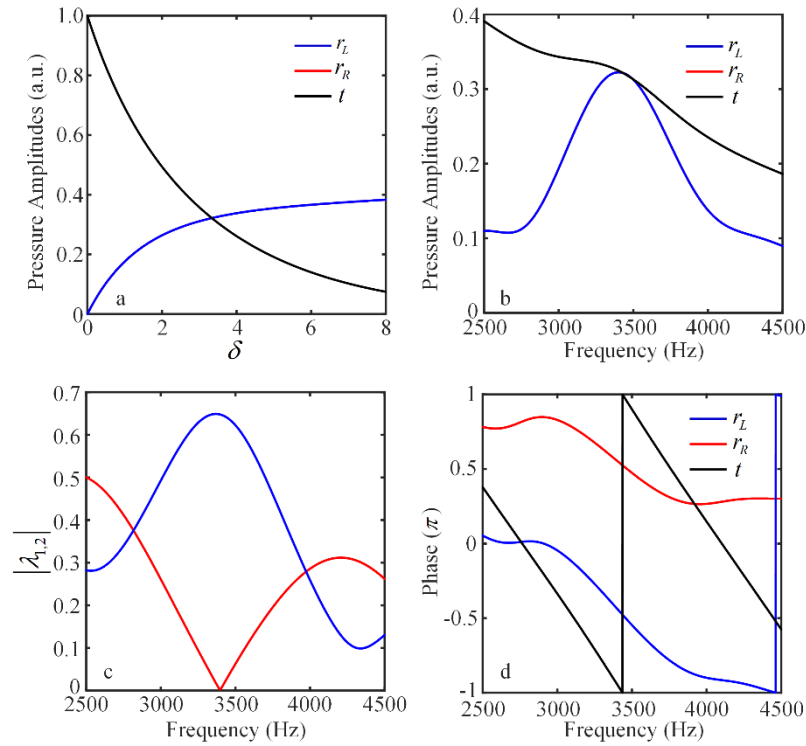


Figure 2| characteristics of the acoustic PT symmetric system. (a) and (b) Pressure amplitudes of the left-(right-) reflected and transmitted waves of the passive PT symmetric system as a function of lossless-loss factor δ and frequency f , respectively. (c) Absolute values of two eigenvalues as a function of frequency. (d) Phases of the left-(right-) reflected and transmitted waves of the passive PT symmetric system as a function of frequency.

We have presented that a well-designed passive acoustic PT symmetric system still possesses physical characteristics of PT symmetry. We further replace the effective lossless and loss media in Fig. 1a with waveguide metamaterial. The mass density and acoustic velocity of the lossless medium A are $\rho_A = 1.21 \text{ kg/m}^3$ and $c_A = 343 \text{ m/s}$, respectively, which are equivalent to the properties of air. Thus, A part modulation is achieved by introducing an acoustic rectangular waveguide without any

decoration. The length and width of the cross section of the rectangular waveguide are $a = 40$ mm and $b = 40$ mm, respectively. For the loss medium B with refractive index $n_B = n_0 - 0.167i$, a deliberate control of sound loss is required. It is known that the resistive boundary can cause the increase of the imaginary part of refractive index, while the real part is almost unchanged. Generally, the attenuation effect can be obtained by the leakage coming from the vent slits. As shown in Fig. 3a, for simplicity, in the full-wave simulation the impedance boundary conditions is directly utilized to describe the upper and lower boundaries of the rectangular waveguides, so that the complex structures can be easily replaced by the effective acoustic impedance homogeneously distributed at the boundaries. Based on the retrieval method of obtaining effective properties of the acoustic metamaterial³⁹, the simulated complex effective refractive indices of the real part (black solid line) and imaginary part (black dotted line) of the loss medium B as a function of boundary acoustic impedance are displayed in Fig. 3b. When the boundary acoustic impedance is $410 \text{ Pa} \cdot \text{s/m}$, the complex refractive index is about $n(x) = 0.95 - 0.161i$. The real part of the effective index is close to 1. Therefore, the passive acoustic PT symmetric material can be constructed by a rectangular waveguide with leakage structures periodically decorated on the waveguide boundaries.

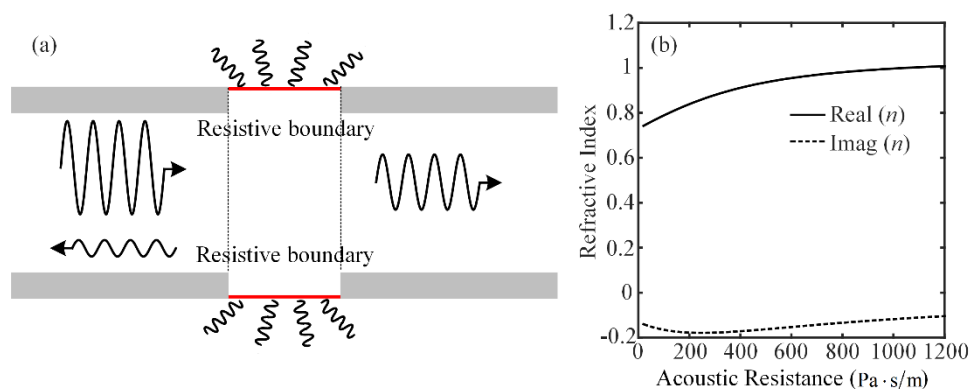


Figure 3| Acoustic metamaterial design for the loss medium. (a) The cross-sectional picture of the acoustic metamaterial for the loss medium. Resistive boundary is equivalent to leakage-structured metamaterial. (b) Simulated complex effective refractive indices of the real part (black solid line) and imaginary part (black dotted line) of the loss medium.

Logic gates and small signal amplifier


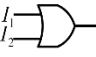
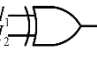
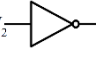
We further numerically simulate the functions of XOR, OR, AND and NOT gates by precisely controlling the phase difference between the two incident beams. The truth tables of all the functions of the acoustic logic gates are presented in Table 1. According to the principle of wave interference

and the transmission and reflection spectra as shown in Fig. 2b, two thresholds A_1 and A_2 are defined to realize all-acoustic logic gates. When the output amplitude is greater than A_1 or A_2 , it corresponds to logic state 1. Otherwise, it corresponds to logic state 0. Here, $A_1 = 0.33p_0$ and $A_2 = 0.65p_0$, where p_0 is the input pressure amplitude of the acoustic beams. For the cases of input states $(p_0, 0)$ and $(0, p_0)$, meaning only one signal beam is injected into left and right ports, respectively. When only one acoustic wave with pressure amplitude p_0 is imposed at left port or right port, the output pressure amplitudes of the left and right sides of the PT symmetric metamaterial are shown in Figs. 4a,b. The simulated results indicate that the output pressure amplitudes of the left port are nearly equal to that of the right port for both cases, which are consistent with the theoretical results. For the case of input state (p_0, p_0) with initial phase difference $\Delta\phi = \pi/2$ at the operating frequency $f = 3430$ Hz, the acoustic waves with amplitude p_0 are simultaneously incident into left and right ports. The corresponding result is illustrated in Fig.4c. When a threshold of $A_1 = 0.33p_0$ is applied, the output logic state 1 responses to input states (p_0, p_0) , $(p_0, 0)$ and $(0, p_0)$ and the proposed device functions as an OR gate. On the other hand, when a threshold of $A_2 = 0.65p_0$ is applied, the output state 1 responses to input state (p_0, p_0) while the output state is 0 for the input states $(p_0, 0)$ and $(0, p_0)$. As a result, the function of AND gate is realized. Furthermore, the XOR gate can be achieved by choosing the initial phase difference $\Delta\phi = -\pi/2$. Figure 4d shows the pressure amplitude distribution under two incident beams with phase difference $\Delta\phi = -\pi/2$ at the operating frequency $f = 3430$ Hz. As shown in Fig. 4d, the output pressure amplitude reaches to 0 in this case. When a threshold of $A_1 = 0.33p_0$ is applied, the output logic state 1 responses to input states $(p_0, 0)$ and $(0, p_0)$, while the output state is 0 for the input states (p_0, p_0) . Therefore, the proposed device can function as a XOR gate. The NOT gate is realized by choosing one of the input ports as a control port with incident pressure amplitude p_0 and using the identical initial phase difference as the proposed XOR gate. Here, the left port is chosen as the control port. As shown in Figs. 4a and 4d, a threshold of $A_1 = 0.33p_0$ is defined. When the right input is turned off, the output logic state is 1 while the output logic state is 0 for the input pressure amplitude p_0 .

Moreover, based on the coherent control effect, the coherent signal amplifier is proposed by the pressure amplitude difference between the two incident beams. By using the same phase difference between two incident beams as the AND logic gate, a small signal amplifier can be realized when the left port is defined as the control port and the right port is defined as the incident

port, as shown in Fig. 4e. As a result, the amplification coefficient for the device is characterized by $O_2/I_2 = 0.34(1/(I_2/I_1) + 1)$. The theoretical result for the coherent signal amplifier is shown in Fig. 4f (black solid curve). When the input signal I_2 is a small signal relative to the control signal I_1 (around $I_2/I_1 < 0.5$), the ratio of output signal O_2 to input signal I_2 is more than 1, which corresponds to the amplification working zone. We refer to this system as the small signal amplifier device. In an extreme case, when $I_2/I_1 = \infty$, O_2/I_2 verges to 0.34. The red triangles in Fig. 4f are the numerical results of coherent signal amplifier, which are consistent with the theoretical results. Therefore, the proposed passive acoustic PT symmetric metamaterial can function as AND, OR, XOR and NOT gates and small signal amplifier without resorting to altering frequency.

Table 1 Truth tables of AND, OR, XOR and NOT gates

Logic Gates		AND	OR	XOR	NOT
I_1	I_2				
1	1	1	1	0	0
0	1	0	1	1	/
1	0	0	1	1	
0	0	0	0	0	/

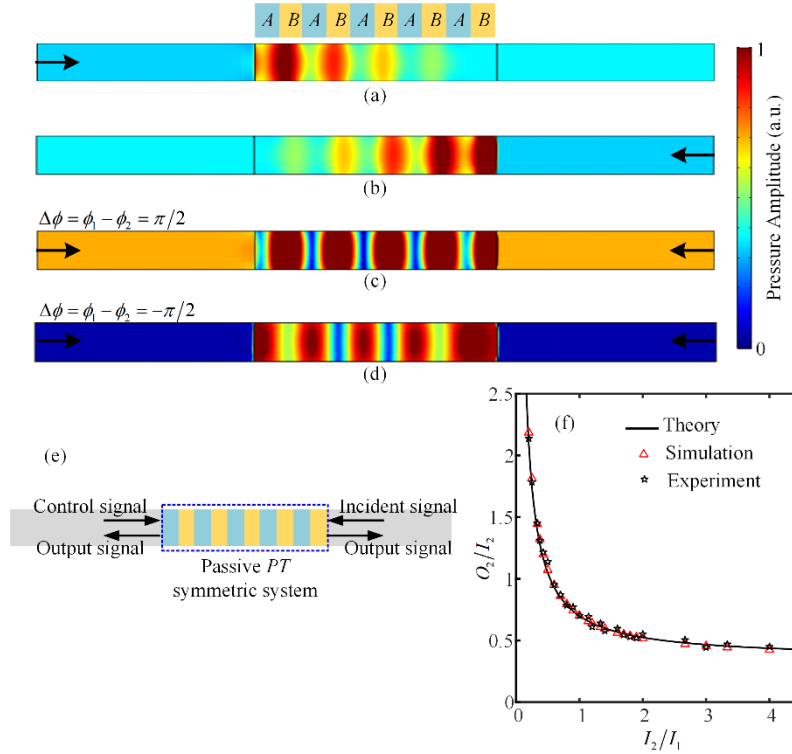


Figure 4| Design and behavior of the acoustic logic gates and amplifier. (a) and (b) Pressure amplitude distributions inside and outside the PT symmetric metamaterial under only one incident wave from left port and right port, respectively. (c) and (d) Pressure amplitude distributions inside and outside the PT symmetric metamaterial under two incident waves with phase difference $\Delta\phi = \pi/2$ and $\Delta\phi = -\pi/2$, respectively. The pressure amplitude distributions outside the metamaterial have subtracted the distribution of incident wave. (e) Schematics of the passive PT symmetric metamaterial for the small signal amplifier. (f) Amplification coefficient O_2/I_2 versus input contrast ratio I_2/I_1 . The black solid line, red triangles and black five-pointed stars represent the theoretical, numerical and experimental results, respectively.

Experimental results

We have theoretically and numerically demonstrated the feasibility of using the passive PT symmetric acoustic metamaterial to design acoustic logic gates and small signal amplifier. In the following, the experimental measurements are performed to verify above theoretical design and simulation results. The set-up of the experiment is shown in Fig. 5a, where the propagating medium of sound wave is air, and sound-absorbing cottons are placed at both ends of the waveguide to eliminate the reflection. Figure 5b is the sample of the passive PT symmetric metamaterial. The same experimental system can realize all the functions of the acoustic logic gates and the small signal amplifier. In our work, two speakers are used to generate the left and right input signals (I_1 and I_2), and the superpositions of the reflected wave and transmitted wave from both sides of the passive PT symmetric metamaterial are treated as output signals (O_1 and O_2). What needs to illustrate is that the acoustic pressures have been normalized in all experimental results. For instance, to have an AND gate, the phase difference of two input waves is set as $\Delta\phi = \pi/2$, and the two states of the speakers' switch (on/off) represent the binary states (1/0). The combination of two input signals demonstrated as Figs. 6a,b goes through all the four input states (1,1), (0,1), (1,0) and (0,0) with time $100 \mu s$. If the threshold value is set to A_2 (black dotted line in Fig. 6c), the left and right output signals of the passive PT symmetric metamaterial present four logic states (1, 0, 0, 0) orderly resembling the AND gate functionality. Similarly, when the phase difference $\Delta\phi = \pi/2$ remains unchanged and another threshold value A_2 (red dotted line in Fig. 6d) is set, the output signals give four different states (1, 1, 1, 0) which function as acoustic OR gate. Another example is that when the phase difference is chosen as $\Delta\phi = -\pi/2$ and the threshold value remains as A_1 (green dotted line in Fig. 6e), the third kind of four output signal states (0, 1, 1, 0) can be achieved, in turn functioning as XOR gate. In a special case, if the threshold value keeps the previous XOR gate condition and

I_1 is set to 1 as the control signal during the whole operation (we pick I_2 as the only input signal; see Figs. 6b1,b3), the corresponding output signal can work as an acoustic NOT gate, as shown in Figs. 6e1,e3. The experimental results of the small signal amplification capability are shown by the black stars in Fig. 4f, which are consistent with the theoretical results (black solid line). The experimental results are consistent with the theoretical and numerical results, indicating that the passive PT symmetric system can successfully act as an acoustic multifunctional device with the capabilities of acoustic logic gates and small signal amplification simultaneously.

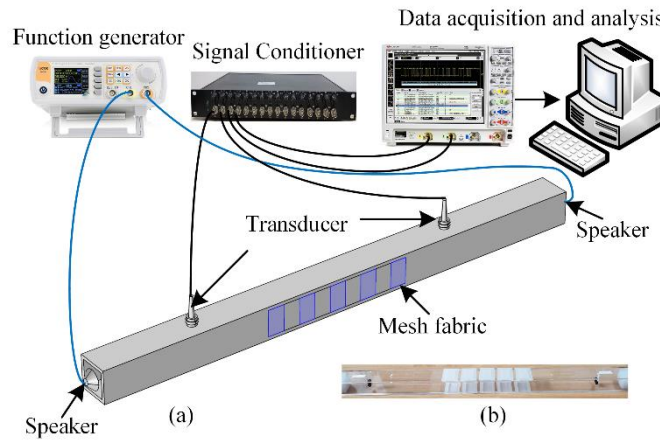


Figure 5| Experimental arrangement and passive PT symmetric metamaterial prototype. (a) Schematics of the experimental arrangement. (b) The photograph of sample fabricated by a rectangular waveguide with leakage structures periodically decorated on the waveguide boundaries. We choose the mesh fabric as the leakage structure. The thickness, average pore and open area of the mesh fabric are $55\mu\text{m}$, $15\mu\text{m}$ and 9%. The effective acoustic impedance of the mesh fabric is about $410\text{ Pa}\cdot\text{s/m}$.

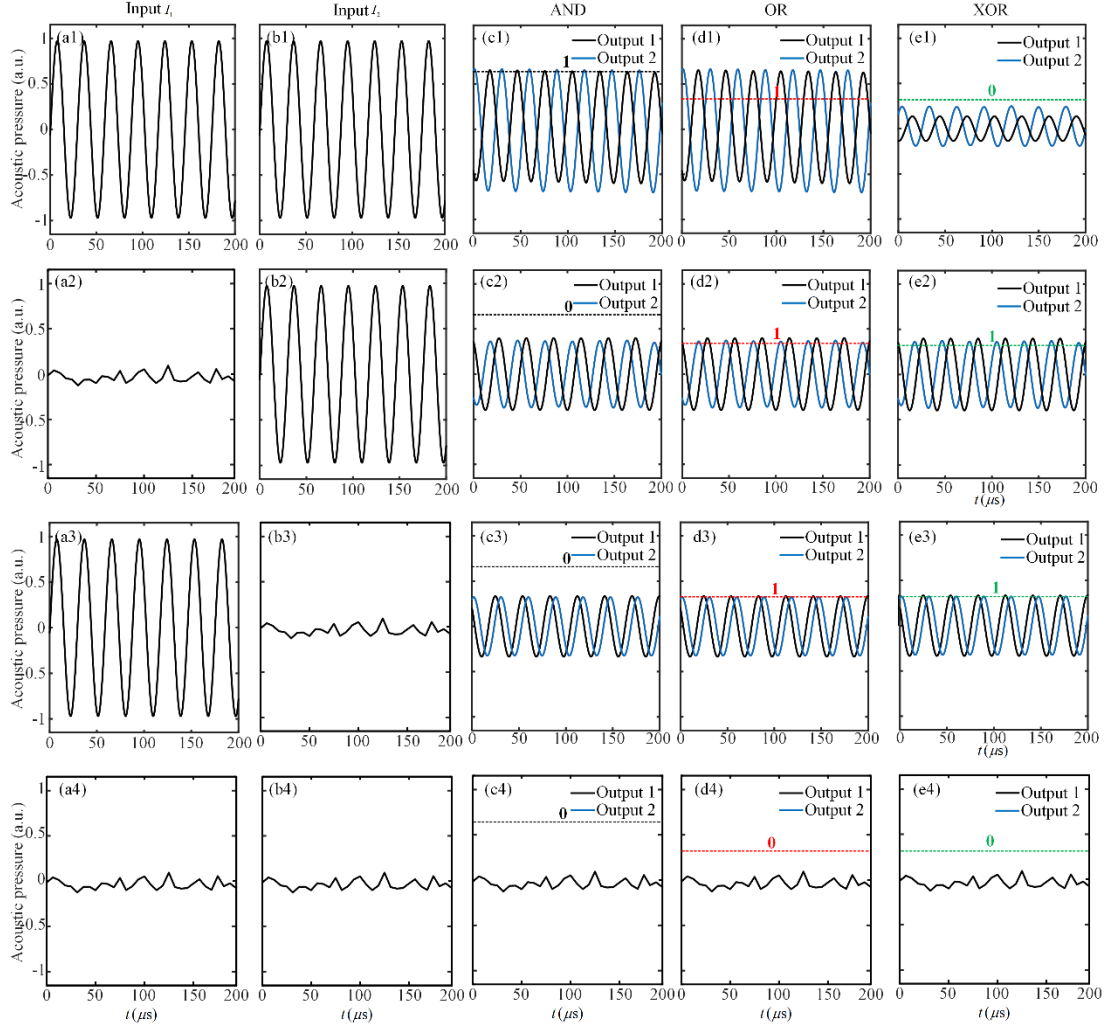


Figure 6| Measured signal for the logic gates of the passive acoustic *PT* symmetric metamaterial at the operating frequency 3430 Hz. (a) and (b) Left and right input signals I_1 and I_2 , respectively. (c), (d), and (e) Left and right output signals O_1 and O_2 for AND, OR, and XOR gates, respectively. The black dashed line in (c) marks the threshold A_2 . The red and green dashed lines in (d) and (e) mark the threshold A_1 .

Discussion

This work presents a realization of a multifunctional device, controlled by *PT* symmetry, which can offer logic gates and small signal amplifier simultaneously without resorting to altering frequency and structure. An efficient and accurate analysis method has been put forward for the design of the passive acoustic *PT* symmetric metamaterial with exotic scattering properties produced by the broken *PT* symmetry phase. Through balancing the interplay between the lossless and loss media, the logic gates and small signal amplifier are realized by controlling the phase and amplitude differences of the input signals, respectively. Further the integration of acoustic delay line enables the phase difference will be accurately controlled and may promise highly integrated acoustic multifunctional devices. This acoustic multifunctional device offers a simple and effective

approach for reducing the integration complexity and signal manipulation in acoustic communication.

References:

1. Wong, Z. J. et al. Lasing and anti-lasing in a single cavity. *Nat. Photon.* **10**, 796-801 (2016).
2. Longhi, S. & Feng, L. PT-symmetric microring laser-absorber. *Opt. Lett.* **39**, 5026-5029 (2014).
3. Silva, A. et al. Performing mathematical operations with metamaterials. *Science* **343**, 160-163 (2014).
4. Boechler, N., Theocharis, G. & Daraio, C. Bifurcation-based acoustic switching and rectification. *Nat. Mater.* **10**, 665-668 (2011).
5. Li, F., Anzel, P., Yang, J., Kevrekidis, P. G. & Daraio, C. Granular acoustic switches and logic elements. *Nat. Commun.* **5**, 5311 (2014).
6. Popa, B. & Cummer, S. A. Non-reciprocal and highly nonlinear active acoustic metamaterials. *Nat. Commun.* **5**, 3398 (2014).
7. Zhang, T., Cheng, Y., Guo, J., Xu, J. & Liu, X. Acoustic logic gates and Boolean operation based on self-collimating acoustic beams. *Appl. Phys. Lett.* **106**, 113503 (2015).
8. Bilal, O. R., Foehr, A. & Daraio, C. Bistable metamaterial for switching and cascading elastic vibrations. *Proc. Natl. Acad. Sci. USA* **114**, 4603-4606 (2017).
9. Liu, Z. et al. Locally resonant sonic materials. *Science* **289**, 1734-1736 (2000).
10. Cummer, S. A., Christensen, J. & Alù, A. Controlling sound with acoustic metamaterials. *Nat. Rev. Mater.* **1**, 16001 (2016).
11. Alagoz, S. & Baykant Alagoz, B. Sonic crystal acoustic switch device. *J. Acoust. Soc. Am.* **133**, 485-490 (2013).
12. Wang, P., Casadei, F., Shan, S., Weaver, J. C. & Bertoldi, K. Harnessing buckling to design tunable locally resonant acoustic metamaterials. *Phys. Rev. Lett.* **113**, 14301 (2014).
13. Bringuier, S. et al. Phase-controlling phononic crystals: realization of acoustic Boolean logic gates. *J. Acoust. Soc. Am.* **130**, 1919-1925 (2011).
14. Bender, C. M. & Boettcher, S. Real spectra in non-Hermitian Hamiltonians having PT symmetry. *Phys. Rev. Lett.* **80**, 5243 (1998).
15. Zhao, H. & Feng, L. Parity-time symmetric photonics. *Natl. Sci. Rev.* **5**, 183-199 (2018).
16. Bender, C. M., Brody, D. C. & Jones, H. F. Complex extension of quantum mechanics. *Phys. Rev. Lett.* **89**, 270401 (2002).
17. Zhu, X., Ramezani, H., Chengzhi, S., Zhu, J. & Zhang, X. PT-symmetric acoustics. *Phys. Rev. X* **4**, 31042 (2014).
18. Rüter, C. E. et al. Observation of parity-time symmetry in optics. *Nat. Phys.* **6**, 192-195 (2010).
19. Li, Y. et al. Anti-parity-time symmetry in diffusive systems. *Science* **364**, 170-173 (2019).
20. Feng, L., El-Ganainy, R. & Ge, L. Non-Hermitian photonics based on parity-time symmetry. *Nat. Photon.* **11**, 752-762 (2017).

21. Shi, C. et al. Accessing the exceptional points of parity-time symmetric acoustics. *Nat. Commun.* **7**, 11110 (2016).
22. Zhu, X. Defect states and exceptional point splitting in the band gaps of one-dimensional parity-time lattices. *Opt. Express* **23**, 22274 (2015).
23. Miri, M. & Alù, A. Exceptional points in optics and photonics. *Science* **363**, 7709 (2019).
24. El-Ganainy, R. et al. Non-Hermitian physics and PT symmetry. *Nat. Phys.* **14**, 11-19 (2018).
25. Zhu, W. et al. Simultaneous observation of a topological edge state and exceptional point in an open and non-Hermitian acoustic system. *Phys. Rev. Lett.* **121**, 124501 (2018).
26. Sakhdari, M., Farhat, M. & Chen, P. PT-symmetric metasurfaces: wave manipulation and sensing using singular points. *New J. Phys.* **19**, 65002 (2017).
27. Lin, Z. et al. Unidirectional invisibility induced by PT-symmetric periodic structures. *Phys. Rev. Lett.* **106**, 213901 (2011).
28. Liu, T., Zhu, X., Chen, F., Liang, S. & Zhu, J. Unidirectional wave vector manipulation in two-dimensional space with an all passive acoustic parity-time-symmetric metamaterials crystal. *Phys. Rev. Lett.* **120**, 124502 (2018).
29. Feng, L. et al. Experimental demonstration of a unidirectional reflectionless parity-time metamaterial at optical frequencies. *Nat. Mater.* **12**, 108-113 (2013).
30. Feng, L. et al. Experimental demonstration of a unidirectional reflectionless parity-time metamaterial at optical frequencies. *Nat. Mater.* **12**, 108-113 (2013).
31. Sun, Y., Tan, W., Li, H., Li, J. & Chen, H. Experimental demonstration of a coherent perfect absorber with PT phase transition. *Phys. Rev. Lett.* **112**, 143903 (2014).
32. Longhi, S. PT-symmetric laser-absorber. *Phys. Rev. A* **82**, 31801 (2010).
33. Zhao, H. et al. Metawaveguide for asymmetric interferometric light-light switching. *Phys. Rev. Lett.* **117**, 193901 (2016).
34. Poshakinskiy, A. V., Poddubny, A. N. & Fainstein, A. Multiple quantum wells for PT-symmetric phononic crystals. *Phys. Rev. Lett.* **117**, 224302 (2016).
35. Jing, H. et al. PT-symmetric phonon laser. *Phys. Rev. Lett.* **113**, 53604 (2014).
36. Feng, L., Wong, Z. J., Ma, R., Wang, Y. & Zhang, X. Single-mode laser by parity-time symmetry breaking. *Science* **346**, 972-975 (2014).
37. Christensen, J., Willatzen, M., Velasco, V. R. & Lu, M. H. Parity-time synthetic phononic media. *Phys. Rev. Lett.* **116**, 207601 (2016).
38. Merkel, A., Romero-García, V., Groby, J., Li, J. & Christensen, J. Unidirectional zero sonic reflection in passive PT-symmetric willis media. *Phys. Rev. B* **98**, 201102 (2018).
39. Fokin, V., Ambati, M., Sun, C. & Zhang, X. Method for retrieving effective properties of locally resonant acoustic metamaterials. *Phys. Rev. B* **76**, 144302 (2007).

Acknowledgements

We acknowledge financial support of the National Key R&D Program (No. 2017YFA0303702),

State Key Program of National Natural Science Foundation of China (No. 11834008), National Natural Science Foundation of China (No. 11774167), State Key Laboratory of Acoustics, Chinese Academy of Science (No. SKLA201809), Key Laboratory of Underwater Acoustic Environment, Chinese Academy of Sciences (No. SSHJ-KFKT-1701) and AQSIQ Technology R&D Program (No. 2017QK125).

Author contributions

J. L. L.W.W and. X. Z. L. developed the theory, performed the numerical simulations (FEM), and prepared the manuscript. M. H. Lu and X. W. Z. contributed to the data analysis. All authors edited the manuscript.

Additional information

Competing Interests: The authors declare that they have no competing interests.